Applications of Polymer, Composite, and Coating Materials

A Self-Repairing, Large Linear Working Range Shape Memory Carbon Nanotubes/Ethylene Vinyl Acetate Fiber Strain Sensor for Human Movement Monitoring

Zhao Li, Xiaoming Qi, Lu Xu, Haohao Lu, Wenjun Wang, Xiaoxiong Jin, Zahidul Islam MD, Yaofeng Zhu, Yaqin Fu, Qing-Qing Ni, and Yubing Dong

ACS Appl. Mater. Interfaces, **Just Accepted Manuscript** • DOI: 10.1021/acsami.0c12425 • Publication Date (Web): 21 Aug 2020

A Self-Repairing, Large Linear Working Range Shape Memory Carbon Nanotubes/Ethylene Vinyl Acetate Fiber Strain Sensor for Human Movement Monitoring

Zhao Li, Xiaoming Qi, Lu Xu, Haohao Lu, Wenjun Wang, Xiaoxiong Jin, MD Zahidul Islam, Yaofeng Zhu, Yaqin Fu , Qingqing Ni, Yubing Dong*

School of Materials Science and Engineering, Zhejiang Sci-Tech University, Hangzhou, Zhejiang, 310018, China

E-mail: dyb19831120@zstu.edu.cn.

ABSTRACT:

Flexible strain sensors have shown great application value in wearable devices. In the past decades, researchers have spent numerous on developing high stretchability, excellent dynamic durability, and large linear working range flexible strain sensors and shaped a series of important research results. However, the viscoelasticity of the elastic polymer is always a big challenge to develop a flexible sensor. Here, to overcome this challenge, we developed a novel self-repairing carbon nanotubes/ethylene vinyl acetate (CNTs/EVA) fiber strain sensors, prepared by embedding the CNTs in the surface of the swollen shape memory EVA fiber via the ultrasonic method. The CNTs/EVA fiber strain sensors responded significant result which has high stretchability (190% strain), large linear working range (up to 88% strain), excellent dynamic durability (5000 cycles), and fast response speed (312 ms). In addition, the permanently damaged conductive network of the strain sensors, caused by the viscoelasticity of elastic polymer, can restore above the transforming temperature of the shape memory CNTs/EVA fiber. Moreover, the performance of the restored strain sensors was almost as same as that of the original strain sensors. Furthermore, terms of human health monitoring tests show that the CNTs/EVA fiber has a broad application prospects for human health monitoring in wearable electronic devices.

KEYWORDS: *strain sensors, self-repairing, large linear working range, carbon nanotubes, ethylene vinyl acetate fiber*

1. INTRODUCTION

The wearable devices have attracted great attention with the gradual popularization of smart products. As the important component of wearable equipment, flexible strain sensors have a great application value in electronic skin, **(1-3)** human movement monitoring, **(4-7)** human-machine interaction, **(8-9)** smart textile. **(10)** To meet the requirements of large recoverable deformation and flexibility simultaneously, flexible strain sensors are generally composed of two units of elastic polymer and conductive fillers. The elastic matrix gives the sensors high stretchability and durability. Currently, commonly used elastic substrates mainly include polydimethylsiloxane (PDMS), **(4,11)** copolyester (Ecoflex), **(12-13)** and thermoplastic polyurethane (TPU). **(7,14)** The conductive fillers used in flexible sensors mainly include carbon-based fillers, conductive polymers, and metal nanowires. **(2,15-19)** Among these conductive fillers, the CNTs have excellent electromechanical properties and their usually in a state of entanglement and bending and the generation of tensile cracks will be reduced to a certain extent after the formation of flexible devices so that the sensors have a broader strain sensing range, which is very adaptive for preparing stretchable flexible strain sensors.

The dynamic durability of flexible strain sensors is an important characteristic of flexible strain sensors because it determines the service life of the strain sensors. In most cases, the deterioration of durability is mainly related to the irreversible deformation of the elastic substrate, the structure of the conductive network, and the weak bonding force between the elastic substrate and the conductive fillers. Currently,

the commonly used elastic polymers matrix (PDMS, Ecoflex, PET, TPU) has an inevitable defect of viscoelasticity, the flexible strain sensors will inevitably appear partially irreversible after underwent multiple cycles of stretching-relaxation due to the viscoelasticity of the elastic polymers, which will be a massive challenge to the dynamic durability and stability of the sensors. Moreover, this irreversible deformation will aggravate with the increase of the number of cycles and lead to the failure of the sensors, which dramatically shortens the service life of the strain sensors. **(20-21)** Wang et al. designed a new flexible strain sensor based on TPU electrospun fibrous mats and reduced graphene oxide (RGO), which found that the RGO/TPU strain sensor had undergone 6,000 stretching-releasing in the 0-50% strain range. The peak value of the relative resistance gradually attenuated as the number of cycles increased. It shows that the dynamic durability of the RGO/TPU strain sensors performance is poor, which limits its application in wearable equipment. **(7)** Huang et al. prepared the CNTs/TPU conductive foam with porous oriented structure and the relative resistance value gradually decayed as the number of cycles increased in the multiple cycles compression-releasing process. The dynamic durability of the CNTs/TPU conductive foam during cyclic compression-releasing was prominently deteriorated. **(22)** Therefore, it is indispensable to prepare flexible strain sensors with a self-repairing function to repair the failure of the sensor caused by fatigue damage and viscoelasticity. Currently, the self-repairing mechanism of flexible strain sensors mainly relies on dynamic (reversible) covalent/non-covalent bonds to achieve self-repairing function. **(23-27)** However, the feasibility of application in wearable electronic devices is hindered by such defects as complicated repair process, long repair time, and low repair efficiency.

Therefore, this is an urgent need to prepare flexible strain sensors with a simple repair process, quick repairing, and high repair efficiency. In recent years, shape memory polymers (SMPs) have been used in sensors, smart textiles, self-repairing, and artificial muscles due to their excellent elasticity, large deformation, and simple manufacturing process. **(28-33)** Compared with shape memory film and shape memory foam, shape memory fiber (SMPFs) have better recovery stress, faster response speed, more excellent mechanical properties, **(34-37)** lightweight, smaller size, and stitchability, which momentously enhances the function of SMPs. **(38-39)** In SMPFs, commercial semi-crystalline EVA has low cost, good elasticity and is easy to process into the fiber. Previous studies have shown that EVA with crystalline and cross-linked structure has the role of melt-induced shrinkage (MIC) under constant and unstressed conditions, which provides the impetus for the self-repairing of SMPFs and the conductive network destroyed by viscoelasticity will be restored after thermal treatment. **(40-43)** Therefore, a flexible fiber strain sensor with shape memory performance is one of the ideal choices in a new generation of wearable devices.

Another reason for deteriorating the dynamic durability of the flexible strain sensors is the weak adhesion between the elastic matrix and the conductive fillers. The researchers used coating method to prepare flexible strain sensors. **(44-47)** Although the strain sensors prepared by the coating method have high conductivity and stretchability due to functional distributed conductive filler on the polymer surface, the repeatability, and dynamic durability of the strain sensors unable to meet the needs of long-term work due to weak binding force between elastic polymer surface and conductive fillers. The interface peeling of the conductive filler on the surface of the conductive composite

material often occurs, which will seriously affect the response of the sensing signal of the strain sensors during the cyclic stretching-relaxing. Therefore, it is still challenging to prepare a comprehensive performance flexible strain sensors with excellent dynamic durability and stability. Recently, the embedded structure is considered to be an effective way to obtain flexible strain sensors with excellent property. **(48-50)** In embedded structure, a perfect conductive network can be formed on the surface of the elastic polymer even at low conductive filler content because conductive fillers are anchored and uniformly embedded in the surface of the elastic polymer. Gu et al. prepared the CNTs-embedded Ecoflex strain sensor with excellent dynamic durability (cycle test of 13000) and good conductivity with CNTs content of only 0.52 wt%. **(51)** Therefore, the inherently high elasticity of the elastic polymer substrate can be retained and resulting in high stretchability and recoverability. Moreover, the embedded structure makes the elastic substrate and conductive filler strongly combined, which endows the strain sensors excellent stability and dynamic durability.

On the other hand, high linearity is an important indicator to evaluate the excellent performance of strain sensors. High linearity means that the signal of the strain sensors will have the same response when the same strain is applied, which is accommodating for the calibration process and circuit design of the entire sensors system. It can be known that the electrical response performance of sensing materials caused by the change of its resistance under external strain. In the case of large deformation, the conductive network of the strain sensors will crack, break, or even damage, resulting in significant changes in the output signal. Therefore, flexible strain sensors are difficult to maintain high linearity over an extensive strain range. There are several strategies to

improve the linear range of strain sensors. **(6)** The linear working range of graphene-based strain sensors is very narrow (about 2%). Yang et al. dropped a mixed solution of graphene oxide and silver nanoparticles uniformly dispersed on a PDMS substrate to prepare strain sensors and the linear working range of the strain sensors was only increased to about 8%. **(4)** Therefore, it is still a challenge to achieve a large working range and high linearity simultaneously.

In this paper, we use the shape memory EVA fiber as the elastic matrix and CNTs as conductive fillers to obtain the CNTs/EVA fiber strain sensors with embedded structure by the swelling-ultrasonic method. The morphology, mechanical property, sensing performance, shape memory property, and self-repairing functions of the CNTs/EVA fiber strain sensors were investigated in detail. Moreover, the human monitoring of the flexible strain sensors was systematically studied and discussed. Besides, the sensing mechanism of the CNTs/EVA fiber strain sensors was also described by the evolution of conductive networks.

2. EXPERIMENTAL SECTION

2.1. Materials. EVA with a vinyl acetate content of 30 wt%, triallyl isocyanurate (TAIC, contains 500 ppm BHT stabilizer), benzophenone (BP, 99 wt%), xylene (99 vol%), N, N-Dimethylformamide (DMF), and Carboxylated (-COOH) CNTs (C139835, diameter=20-30 nm, length=10-30 μm) was purchased from Aladdin Reagent, China. All the chemicals were used as received.

2.2. Preparation of EVA Fiber. The fabrication process of the pure EVA fiber was shown in **Figure 1a**. EVA, TAIC, and BP were mixed at a mass ratio of 90: 5:

5. The temperatures of the extruder heating zone were set to 85 °C, 90 °C, 95 °C and 100 °C. Then, the mixture is melt-extruded by a micro twin-screw extruder. (SJSZ-10A, Wuhan Ruiming, China) and the EVA fibers are collected by collecting rollers. EVA fiber was separated from the collecting roller and irradiated under UV lamp for 3 h.

2.3. Preparation of CNTs/EVA Fiber Strain Sensors. The fabrication process of the CNTs/EVA fiber strain sensors were illustrated in **Figure 1b**. Firstly, EVA fiber was soaked in 100 mL xylene solution at 40 °C for 30 min. Because of the diffusion of xylene into EVA fiber, the volume of EVA fiber increased dozens of times. Subsequently, 100 mg (-COOH) CNTs were dispersed in a mixed solution of 20 mL DMF and 80 mL deionized at a temperature of 0 °C and sonicated for 10 min by probe ultrasonic machine. And then we got a homogeneous CNTs solution. The swollen EVA fiber was immersed in the homogeneous CNTs solution under ultrasonic for 10 min. Then, the CNTs/EVA fiber was rinsed several times with deionized water to remove not well adhered CNTs. The volume of CNTs/EVA fiber returned to its original size after drying in the air for 24 h at room temperature. The copper sheet was bonded to two ends of the CNTs/EVA fiber and the distance between the two ends of the electrode was 20 mm.

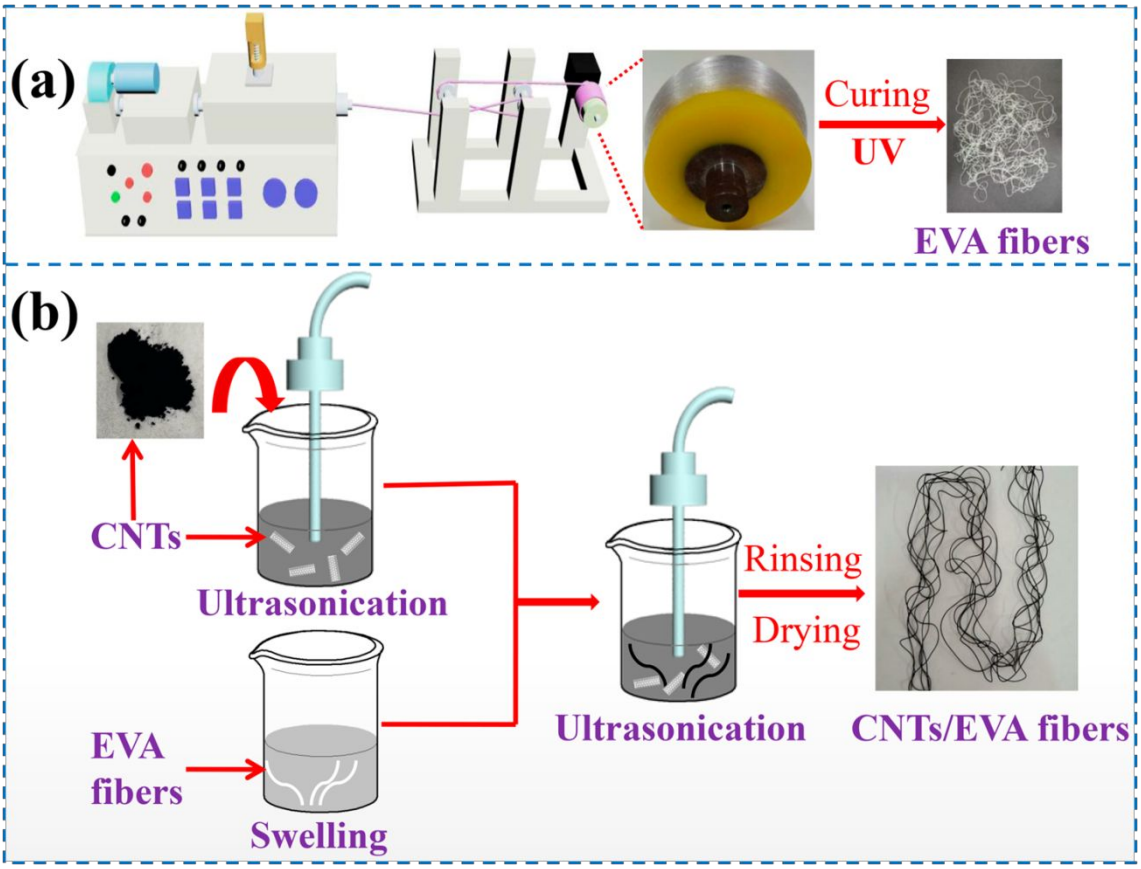

Figure 1. (a) Schematic illustration of the fabrication process of pure EVA fiber. (b) Schematic illustration of the fabrication process of CNTs/EVA fiber.

2.4. Characterization. The surface and cross-sectional SEM images of the sample were observed using scanning electron microscopy (FE-SEM). The mechanical properties of the pure EVA fiber and the CNTs/EVA fiber were tested by the multifunction tensile tester (KES-G1, Kato Tech Co, Japan) at 10 mm/min.

The current (I)–voltage (V) relationship was investigated by using RST5200 electrochemical workstation. The electrometer (Keithley 6514) was combined with the multifunction tensile tester to record the real-time resistance of the CNTs/EVA fiber in the tensile state. The sensitivity of CNTs/EVA fiber strain sensors were evaluated by the gauge factor (GF), as shown in the following formula: $GF= ((R-R_0)/R_0)/\varepsilon$, where R is the resistance under stretching, R_0 is the initial resistance, and ε is the applied strain.

The thermal characteristics of the pure EVA fiber and the CNTs/EVA fiber were evaluated by differential scanning calorimetry (DSC Q2000, TA Instruments, America) and thermogravimetric analysis (TGA Pyris 1, Perkin Elmer, America). The shape memory effect of the CNTs/EVA fiber was tested by the thermomechanic analyzer (TMA Q400, TA Instruments, America) in the stretched mode. According to the thermo-mechanical test results, two main parameters for quantitatively characterizing the shape memory property of samples can be obtained through the following formulas (1) and (2): shape fixity ratio (R_f) and shape recovery ratio (R_r) used to quantify the memory capacity of the temporary shape and the recovery ability of the permanent shape, respectively.

$$R_f = \frac{\varepsilon_{unload} - \varepsilon_{inital}}{\varepsilon_{load} - \varepsilon_{inital}} \times 100\% \quad (1)$$

$$R_r = \frac{\varepsilon_{unload} - \varepsilon_{rec}}{\varepsilon_{unload} - \varepsilon_{inital}} \times 100\% \quad (2)$$

In equations (1) and (2), $\varepsilon_{\mathrm{unload}}$ is the strain after the stress is removed from the sample, $\varepsilon_{\mathrm{inital}}$ is the initial strain with the thermal history removed, $\varepsilon_{\mathrm{load}}$ is the maximum strain of the sample after the stress is applied, and $\varepsilon_{\mathrm{rec}}$ is the strain of the sample after reheating and shape recovery. In terms of human motion monitoring, the CNTs/EVA fiber strain sensors were directly adhered to the surface of the skin by medical tape to monitor the relative resistance under different motion states.

3. RESULTS AND DISCUSSION

3.1. Morphology.

Figure 2 shows the surfaces and cross-section SEM images of the pure EVA fiber

and the CNTs/EVA fiber. As shown in **Figure 2a-c**, the surface and cross-sectional of the pure EVA fiber is smooth. The CNTs are well distributed on the EVA fiber surface and the surface of the CNTs/EVA fiber is crumpled after swelling-ultrasonic treatment (**Figure 2d-e**). We can see some CNT embed in the surface of the EVA fiber (solid red cycle in **Figure 3f**) and some CNT in semi-insertion state, one end of the CNTs insert into the substrate or entangle with other CNTs, and the other end of CNT is exposed (red dotted red circle in **Figure 3f**). According to cross-sectional SEM images of the CNTs/EVA fiber (**Figure 2g-2i**), the EVA fiber is well covered with layer of CNTs, and the CNTs are compactly combined with EVA fiber (**Figure 2i**), which can be known from **Figure S1** and the ultrasonic mechanism. **(7,52)** The three-dimensional conductive pathways are observed on the surface of the CNTs/EVA fiber. It is shown that the conductive network of the CNTs/EVA fiber is composed of two parts. The first is composed of CNTs on the surface of EVA fiber overlapping each other and the second consists of CNTs embedded in EVA fiber. The anchoring effect of the embedded structure makes the CNTs network have the same deformation as the EVA fiber substrate, which creates outstanding recoverable deformed conductive network of the CNTs/EVA fiber. This laid the foundation for the stability and excellent dynamic durability of the CNTs/EVA fiber.

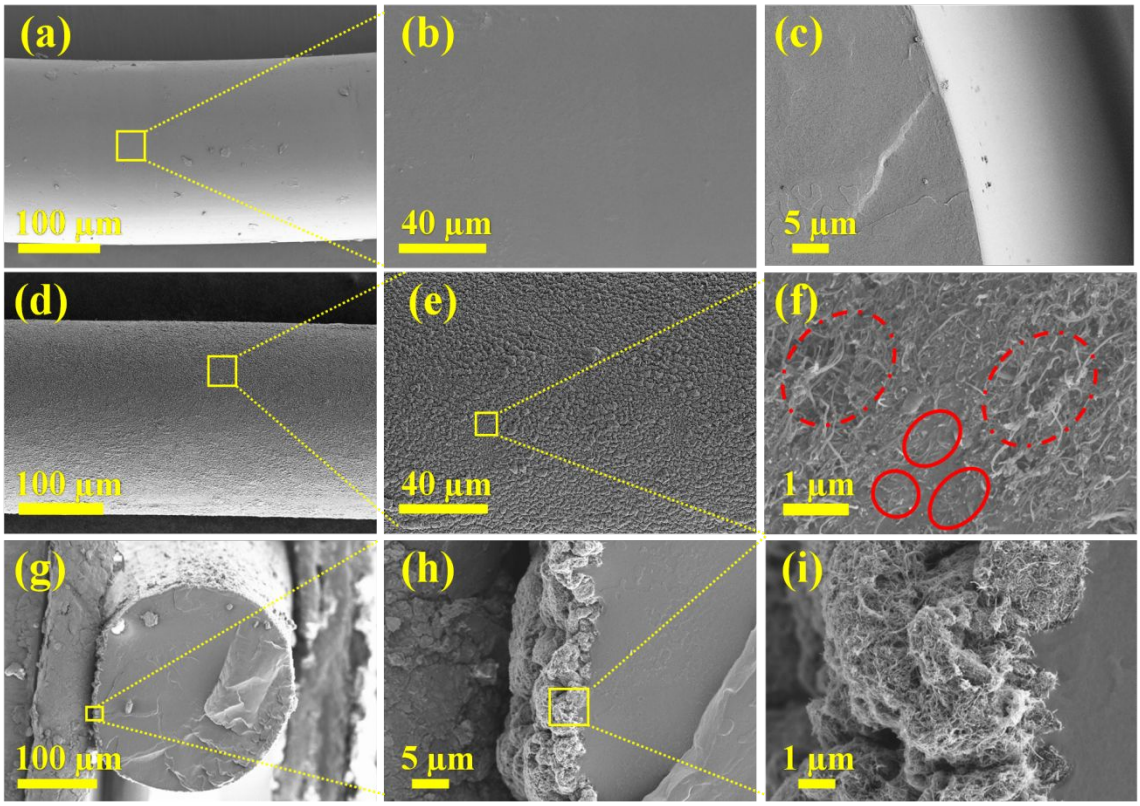

Figure 2. SEM images of the pure EVA fiber and CNTs/EVA fiber. (a-b) Surface morphologies of pure EVA fiber. (c) Cross-section morphologies of pure EVA fiber. (d-f) Surface morphologies of CNTs/EVA fiber. (g-i) Cross-section morphologies of CNTs/EVA fiber.

3.2. Mechanical Properties.

Figure 3a-d shows that the CNTs/EVA fiber has excellent deformability. The mechanical properties of the sample are the critical factor in application of the strain sensors. It is seen from **Figure 3e-f**, the pure EVA fiber and the CNTs/EVA fiber have similar mechanical behavior. Besides, both have an enormous elongation at break and high tensile strength. Compared with the pure EVA fiber, the tensile strength and the elongation at break of the CNTs/EVA fiber improved slightly. On the one hand, the thickness of the CNTs layer is very small compare with the radius of the EVA fiber (as shown in **Figure 2g-h**). On the other hand, there are only small parts of the CNTs

embedded in the EVA fiber, and almost CNTs are entangle with each other on the surface of the EVA fiber (as shown in **Figure 2f**). Therefore, the CNTs layer has a little effect on the mechanical reinforcement of the EVA fiber. The mechanical properties and deformability of the CNTs/EVA fiber provide a guarantee for its application in wearable electronics.

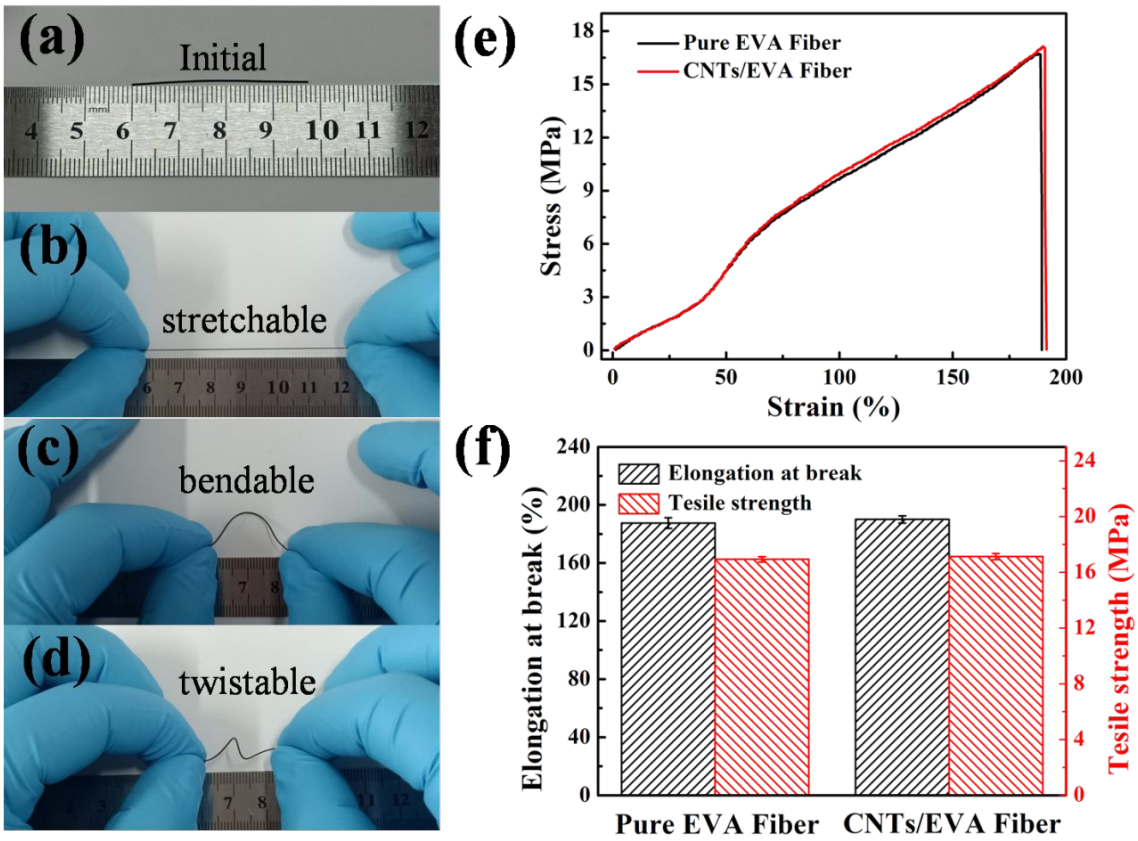

Figure 3. (a-d) Photographs of CNTs/EVA fiber at different states. Mechanical performances of pure EVA fiber and CNTs/EVA fiber: (e) stress-strain curves. (f) tensile strength and elongation at break.

3.3. Electrically conductive property and stability of CNTs/EVA fiber.

As can be seen from **Figure 4a**, the conductivity of the CNTs/EVA fiber gradually increased with the extension of the ultrasonic time. This can be explained that the

number of CNTs embedded in the EVA fiber increases, increasing the conductive path and conductive network more perfect. The electrical conductivity of the CNTs/EVA fiber change is not apparent when the ultrasonic time exceeds 10 min, showing perfect and steady conductive networks had been formed, and increasing the ultrasound time will hardly affect the conductivity. Therefore, the CNTs/EVA fiber with ultrasound for 10 min was selected for sensors performance study. The steady and high conductivity of the CNTs/EVA fiber helps them to output stable signal as strain sensors.

In order to study the stability of the bonding between CNTs and EVA fiber, the CNTs/EVA fiber was placed in deionized water for ultrasonic treatment and compares the clarity of the DI water before and after 5 min treatment, then dried at room temperature for 12 h to measure electrical conductivity. After the CNTs/EVA fiber was sonicated in deionized water for 5 min, the deionization was still very clear, which showed that there was not a large amount of CNTs falling off the EVA fiber and confirms the strong adhesion between CNTs and EVA fiber (as shown Video 1). It can be seen from **Figure 4b** that after 30 minutes of ultrasound, the relative conductivity of the CNTs/EVA fiber only increased by 15.89%. When the ultrasonic time exceeds 30min, the relative conductivity of the CNTs/EVA fiber is hardly affected by the ultrasonic time, indicating that strong bonding between CNTs and EVA fiber and this is of great significance to the excellent dynamic durability of the CNTs/EVA fiber, which can be explained by the mechanism of ultrasound.

The CNTs content of the CNTs/EVA fiber and the fiber thermal stability were investigated by TGA. The following relationship exists in the thermal decomposition

process.

$$m_g + m_p = m_t \quad (3)$$

$$m_g + a \cdot m_p = b \cdot m_t \quad (4)$$

$$w_g = \frac{m_g}{m_t} = \frac{b-a}{1-a} \quad (5)$$

In equations (3), m_g and m_p represent the weight of CNTs and EVA fiber in the CNTs/EVA fiber, respectively. The total weight of the CNTs/EVA fiber is m_t. a and b represent the residual weight percentage of the pure EVA fiber and the CNTs/EVA fiber after thermal decomposition, respectively. According to equations (5), the weight fraction w_g of CNTs in the CNTs/EVA fiber can be calculated. As shown in **Figure 4c**, when the EVA fiber and the CNTs/EVA fiber were degraded at 700 °C, the weight fraction of the residual material was 0.526% and 1.892%, respectively. Substitute it into the equations (5) and w_g is calculated as about 1.37 wt%. In addition, the TGA curve of the CNTs/EVA fiber shifted toward to the high-temperature region compared with the pure EVA fiber and the temperature of the maximum thermal weight loss rate increased from 495.4 °C to 503.5 °C (**Figure 4d**), indicating that the embedding of CNTs enhanced the thermal stability of the EVA fiber. Similar phenomena have been reported in other conductive polymer composites. **(53)** The excellent distribution of CNTs in the surface of EVA fiber and the strong adhesion between the CNTs and the substrate of EVA fiber is crucial to improve the thermal stability. The CNTs hit the EVA fiber with high energy and breakneck speed during ultrasonic treatment. Besides, the EVA fiber softened or melted at the impact site, so that the CNTs was tightly and firmly attached to the EVA fiber, and finally formed a conductive fiber with strong interaction

embedded structure.

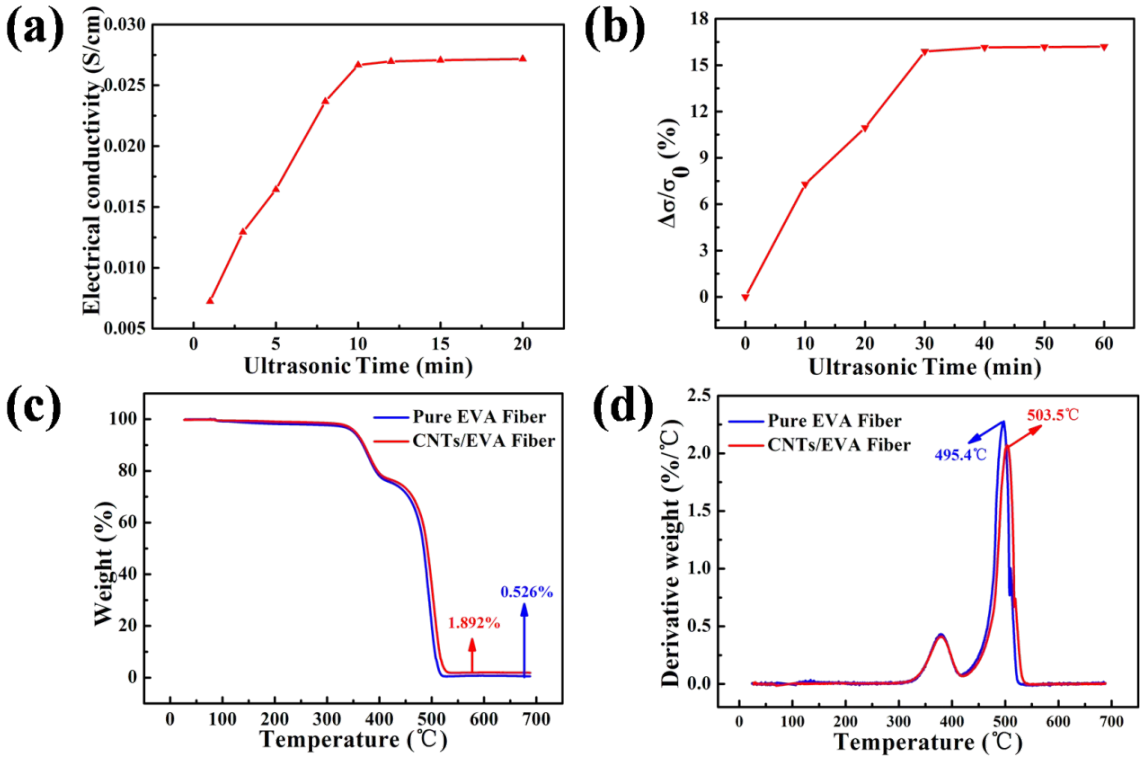

Figure 4. (a) The conductivity of CNTs/EVA fiber with different ultrasonic time of swollen EVA fiber in the uniformly dispersed CNTs solution. (b) The conductivity of CNTs/EVA fiber with different ultrasonic times in deionized water. (c-d) TGA curves of pure EVA fiber and CNTs/EVA fiber.

3.4 Strain Sensing Behavior.

The strain sensing property of the CNTs/EVA fiber will be evaluate, which can be seen from **Figure 5a**, the relative resistance of the CNTs/EVA fiber increases with increasing the applied strain and the relative resistance is typically correlated with the strain in the range of 0-190%. In uniaxial stretching, the CNTs must maintain the same deformation as the EVA matrix, increasing in the distance between the CNTs and a reduction in the area of the area where the CNTs overlap each other, which causes the

relative resistance of the CNTs/EVA fibers to increase. Besides, the CNTs conductive network is destroyed when the strain reaches 190%, which can be explained by the fact that the CNTs/EVA fiber have broken at 190% strain. This unique relationship between strain and relative resistance can be beneficial in distinguishing external strain. In order to further investigate the performance of the CNTs/EVA fiber strain sensors, the GF is used to evaluate the sensitivity of strain sensors. It can be seen from **Figure 5a**, the strain sensing range can be divided into two stages. In the first stage (0-88% strain), the relationship between relative resistance and strain exhibits an ideal linear relationship (R^2=99.5%), which is of great help to the calibration process and circuit design of the entire sensing system. The GF in the second stage (88-190% strain) is much larger than that of the GF in the first stage, indicating that the CNTs conductive network was more severely destructed than the first stage. Our CNTs/EVA fiber strain sensors exhibit high sensitivity (33.29) and extensive linear strain range (190%). The CNTs are anchored on the surface of the fiber and can only be deformed together with EVA fiber so that GF is highly stable over the full range.

The schematic of relative resistance change of the CNTs/EVA fiber is illustrated in **Figure 5b**, the conductive network of the CNTs/EVA fiber is composed of two parts of CNTs (conductive network of CNTs embedded in EVA fiber and conductive network of semi-inserted CNTs on the surface of EVA fiber). In the unstretched state, CNTs are tightly connected like islands to form a perfect conductive network (**Figure 5c**). As the fiber is stretched, its diameter shrinks. CNTs not only shrink in the transverse direction, but also oriented along the stretching direction. However, the degree of orientation of CNTs along the stretching direction is greater than the contraction in the transverse

direction. Therefore, from the overall effect, the separation of the island-shaped CNTs on the surface of the CNTs/EVA fiber in the vertical stretching direction and the CNTs produce distinct orientation along the stretching direction under 90% strain, resulting in clearly visible groove-lines in **Figure 5d.** This further shows that the CNTs are firmly anchored to the EVA fiber surface, because CNTs must be oriented along the stretching direction as the EVA fiber deforms. And this phenomenon is consistent with the schematic diagram shown in **Figure 5b.** Meanwhile, when the strain reaches about 90%, the orientation of the CNTs on the EVA fiber surface reaches the maximum and it can be seen from **Figure 5e** that many broken hooks appear on the groove-line along the orientation direction, which causes a sudden change in the conductive network. Therefore, the relative resistance has a sudden change in **Figure 5a**. The above reasons cause the relative resistance to increase with strain. More interestingly, the resistance is almost completely restored due to the embedded structure and good elasticity of the EVA fiber after removing stress.

To evaluate the long-term dynamic durability of the CNTs/EVA fiber strain sensors. The CNTs/EVA fiber was subjected to cyclic stretching-releasing test under 30% strain at 100 mm/min for 5000 cycles. It can be seen from **Figure 5f**, the CNTs/EVA fiber continues to output a stable relative resistance response. The inset figure of **Figure 5f** shows that the relative resistance cannot fully recovered in the first few cycles due to the viscoelasticity of the CNTs/EVA fiber. However, after several destructions and reconstructions of the conductive network, the relative resistance of CNTs/EVA fiber tends to be stable, indicating that the CNTs/EVA fiber has excellent dynamic durability and repeatability. These characteristics are caused by the embedded

conductive network formed by the strong interaction between CNTs and EVA fiber and the excellent elasticity of the CNTs/EVA fiber.

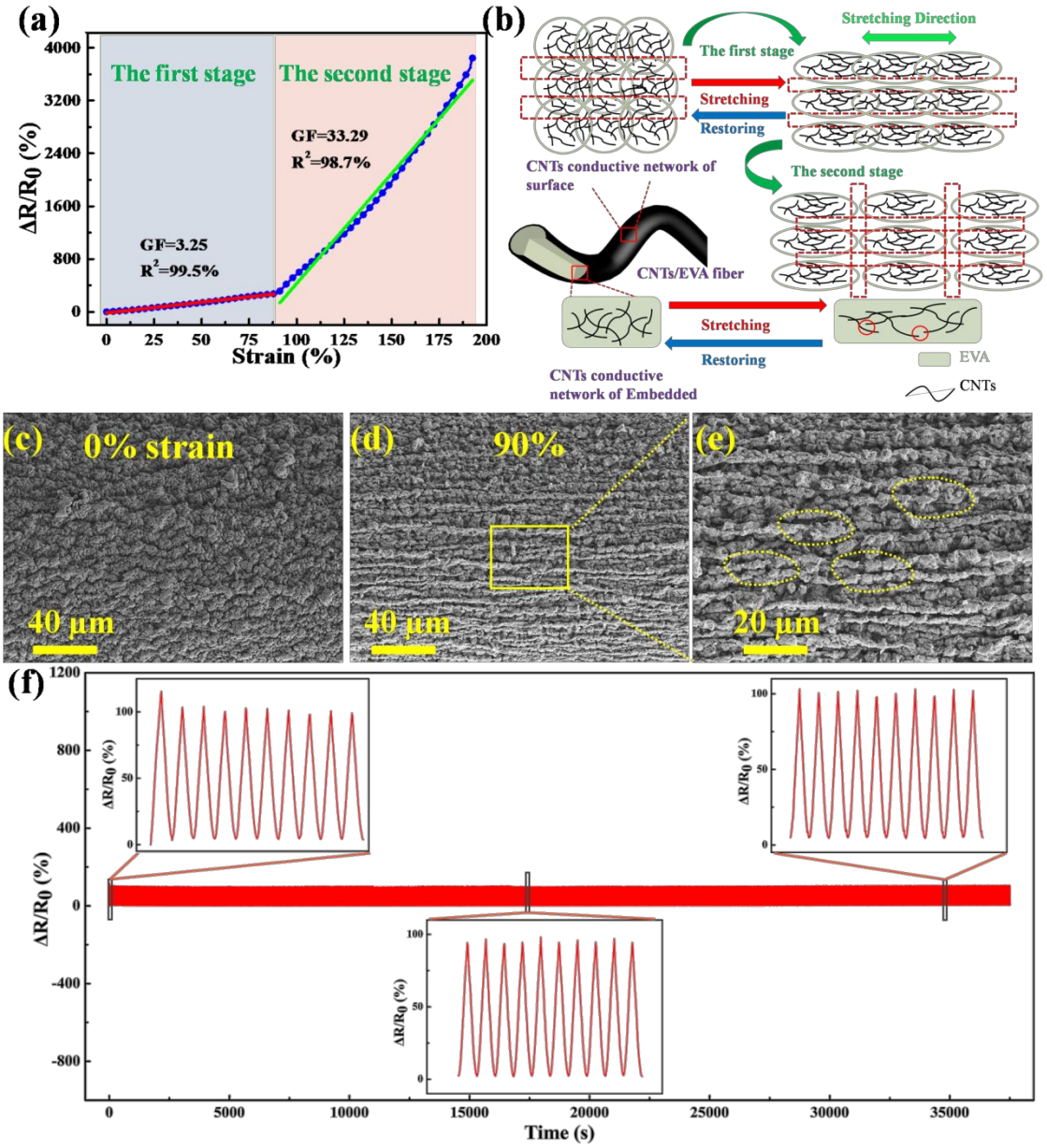

Figure 5. (a) The relative resistance change of CNTs/EVA fiber strain sensors vs strain. (b) Illustration of the mechanism of CNTs/EVA fiber conductive network changes at the stretched state and unstretched state. (c) SEM image of CNTs/EVA fiber in unstretched state. (d-e) SEM image of CNTs/EVA fiber under 90% strain. (f) Cyclic stretching-releasing of CNTs/EVA fiber sensors under 30% strain at 100 mm/min for

5000 cycles. The insets in (f) show enlarged plots of 1-10 cycles, 1330-1340 cycles, and 4660-4670 cycles, respectively.

Figure 6a shows the stability of dynamic resistance of the CNTs/EVA fiber, which was tested by cyclic stretching-releasing under different strains (5, 10, 20, 30, 40, and 50%) at 30 mm/min. The signal response of the CNTs/EVA fiber is consistent under the same strain, which is because the conductive network of the CNTs suffered the same degree of damage at the same strain. The maximum value of the relative resistance of the CNTs/EVA fiber increases with the increasing strain, which is due to reduced contact points and increased distance between CNTs. This characteristic endows the CNTs/EVA fiber the ability to monitor different actions, which is an essential feature in practical application.

The relationship of the strain and relative resistance versus time at a range of 0-60% is shown in **Figure 6b**. The relative resistance and the cyclic strain curves almost completely match during the cyclic stretching-relaxing process. The relative resistance returns to the original value when the stress is removed, which confirms that the relative resistance is reversible and repeatable during the cyclic stretching-relaxing. Besides, the instantaneous synchronous curve of relative resistance with strain indicates that the CNTs/EVA fiber strain sensors have a faster response to the external strain, ensuring simultaneous monitoring of deformation. Moreover, as shown in **Figure 6c**, the CNTs/EVA fiber was tensile tested at different tensile rates in 30% strain. The resistance increased during the loading process and recovered well during the unloading process because of the embedded structure of the CNTs/EVA fiber (**Figure 2f**).

Interestingly, the maximum value of the relative resistance remains stable and consistent under different tensile rates. It is shown that the change of relative resistance of the CNTs/EVA fiber strain sensors is only related to the strain but hardly affected by the tensile rate, which is beneficial to obtain reliable response signal under different external stimuli.

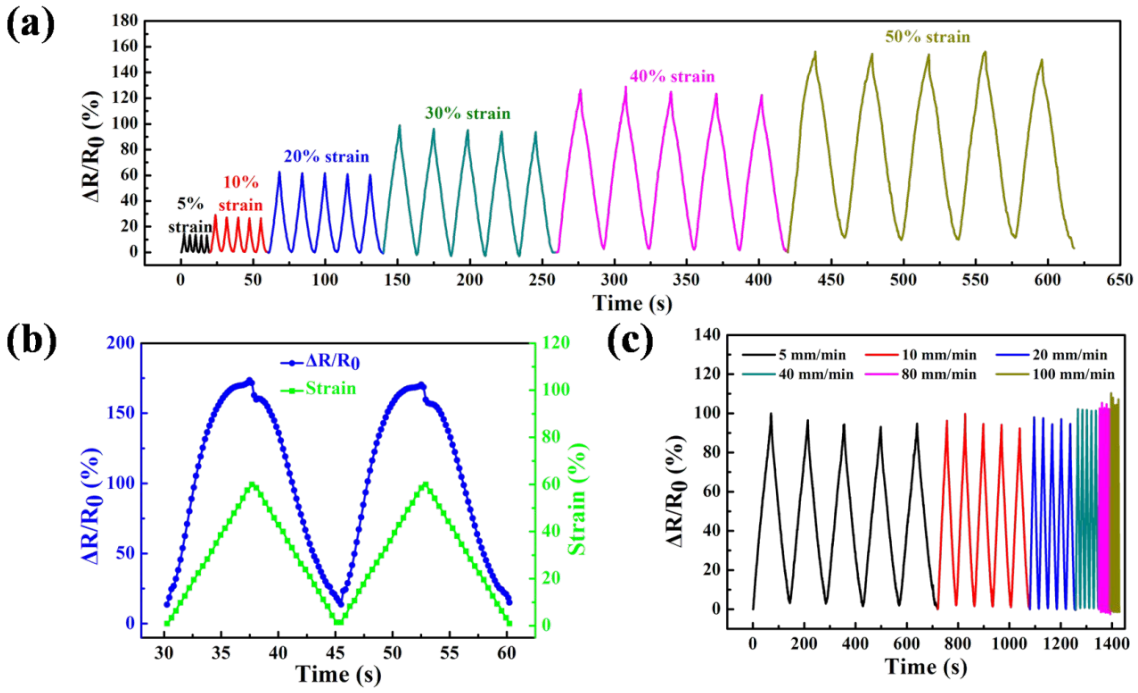

Figure 6. (a) The relative resistance changes of CNTs/EVA fiber with different strains at 30 mm/min. (b) The strain and relative resistance vs time between 0 and 60% strain at 100 mm/min. (c) The relative resistance change of CNTs/EVA fiber under 30% strain at a tensile rate of 5, 10, 20, 40, 80, and 100 mm/min.

Furthermore, as shown in **Figure 7a**, the CNTs/EVA fiber is applied to a strain from 0% to 35% and then to 0% in 5% increments. The relative resistance gradually increases due to the separation between CNTs and the reduction of contact points when the applied strain increases. The relative resistance of the strain sensors has a small attenuation during the residence period. This is because the destruction of the CNTs

conductive network stop immediately and the reconstruction of the CNTs conductive network still exist when the CNTs/EVA fiber is maintained at a particular strain so that the relative resistance value has a slight drop. However, the reconstruction of the CNTs conductive network ceased with time and the relative resistance decreased slightly and tended to stabilize. Similar phenomena have been reported in other flexible strain sensors. **(54)** The CNTs contact joint is rebuilt and the relative resistance is restored when the strain is released from 35% to 0% due to the unique embedded structure and good elasticity of the EVA matrix. Consistent and continuous response curves show the CNTs/EVA fiber with excellent stability and recoverability is suitable for human health monitoring.

The static resistance stability of the CNTs/EVA fiber under different strains was studied. **Figure 7b** shows the I-V curves of the CNTs/EVA fiber under different strains. It can be observed that the CNTs/EVA fiber with different applied strain displays the good linear relationship between current and voltage in the interval from -1V to 1V, which proves that the CNTs/EVA fiber conforms to ohm law under different strains. In addition, with the increase of strain load, the slope of the obtained I-V curve gradually decreases, indicating that the resistance of the CNTs/EVA fiber increased monotonically with strain increasing. These results indicate that the CNTs/EVA fiber show excellent static resistance stability under different strains, which is a potential application in monitoring human movement.

Response time is another important index to evaluate the performance of the strain sensors. The CNTs/EVA fiber was stretched to a tiny strain (1% strain) in a high tensile

rate (500 mm/min) and maintained for 20 s, and then restored to its original position at the same rate as shown in **Figure 7c**. According to **Figure 7d-e**, the response time and recovery time of the CNTs/EVA fiber were 312 ms and 327 ms, respectively. The short response time can ensure that the strain sensors can accurately and quickly detect the response signal when it is stimulated by rapidly changing external movement, which is very important in practical applications. The strong combination of CNTs and EVA fibers in the embedded conductive network structure is beneficial to directly promote the CNTs network to change with the deformation of EVA fibers, which creates a fast response speed of the CNTs/EVA fiber.

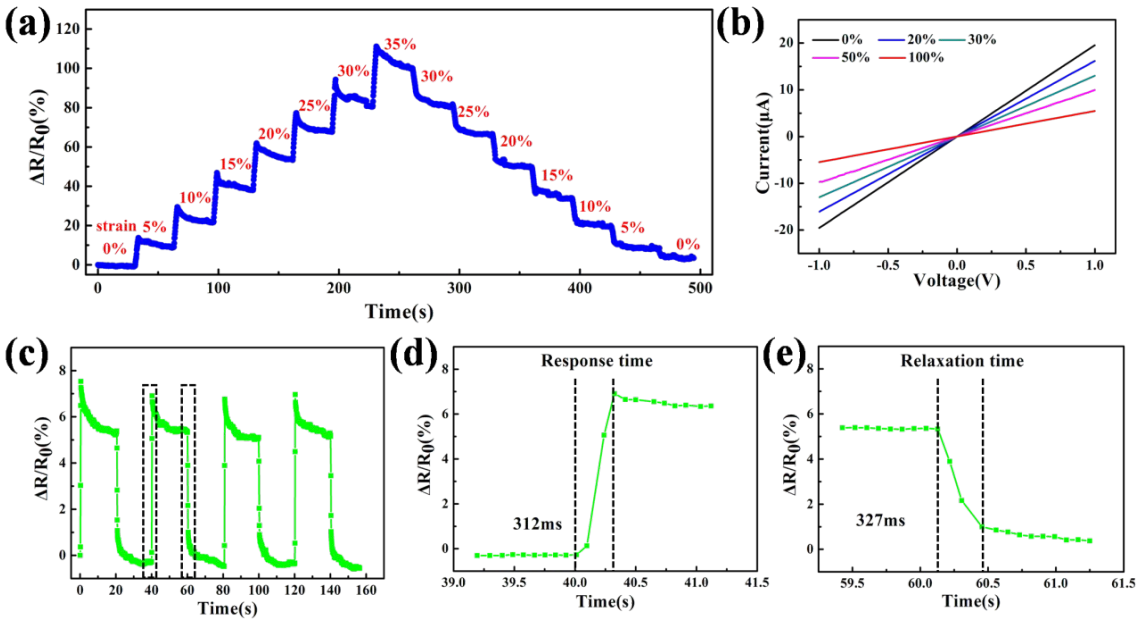

Figure 7. (a) The relative resistance change of CNTs/EVA fiber vs strain from 0% to 35% and then to 0% in 5% increments. (b) Current-voltage characteristic of CNTs/EVA fiber strain sensors curves under various strains (0, 20, 30, 50, and 100%). (c-e) Response time and relaxation time of CNTs/EVA fiber strain sensors.

3.5. CNT/EVA Fiber Viscoelasticity.

Figure 8a shows the change in relative resistance is synchronized with the strain during stretching-releasing. Although the relative resistance cannot be restored to its original value after the stain returns to zero in the first cycle, the relative resistance will return to a valley value and achieve stability in subsequent cycles. The viscoelasticity of CNTs/EVA fiber caused residual strain (**Figure 8e**), which caused partial permanent damage to the CNTs conductive network. Therefore, the relative resistance cannot be completely restored to the original value in the first cycle (**Figure 8b**). Although 10% of the residual strain is retained during the first stress-strain cycle, the stress-strain hysteresis effect becomes weaker after the first cycle (**Figure 8f-g**), indicating that the network of the CNTs/EVA fiber has been adjusted and perfected after the first cycle tensile test. Eventually, the conductive paths tend to stabilize and the relative resistance can return to its original value (**Figure 8c-d**), which is beneficial to the practical application of the CNTs/EVA fiber.

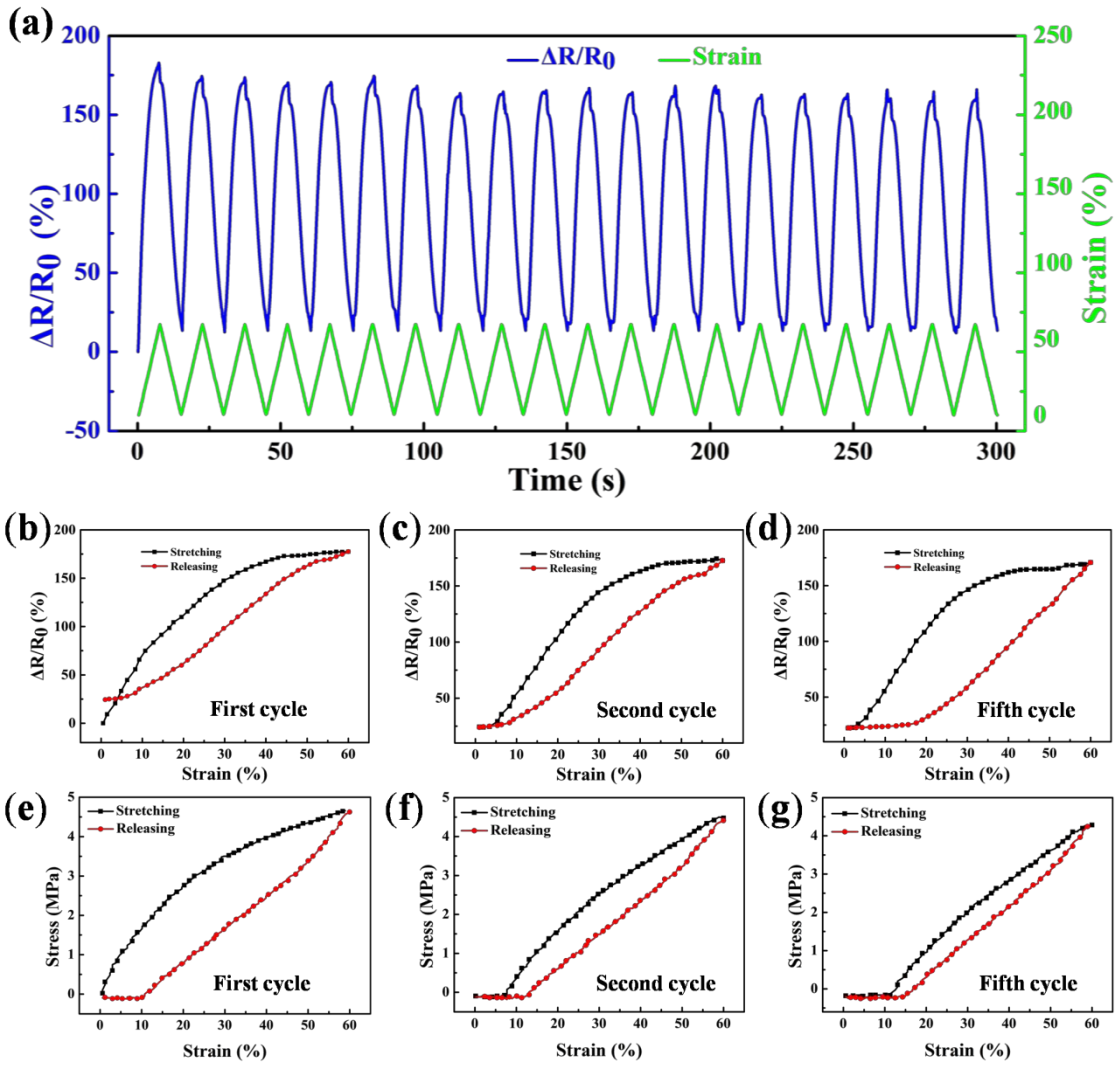

Figure 8. (a) The strain and relative resistance vs time between 0 and 60% strain at 100 mm/min. (b-d) Curves of strain vs relative resistance of first, second and fifth cycles. (e-g) The stress vs strain curves of the first, second and fifth cycles.

3.6. CNTs/EVA fiber repairability.

The thermal properties of the CNTs/EVA fiber were investigated via DSC. As can be seen from **Figure 9a**, The CNTs/EVA fiber exhibited obvious melting and crystallization behavior, and the melting temperature (T_m) and crystallization temperature (T_c) are approximately 65.8 °C and 40.2 °C, respectively. The thermal repair performance of CNTs/EVA fiber depends on the melt-induced contraction of the

CNTs/EVA fiber under constant stress and stress-free conditions. Therefore, when the thermal repair temperature is slightly higher than T_m, the melting-induced contraction of the CNTs/EVA fiber will drive the recovery of the permanently damaged conductive network caused by viscoelasticity, thus achieving self-repairing function. In addition to studying the thermal properties of the CNTs/EVA fiber, the shape memory properties of the CNTs/EVA fiber were investigated by TMA in dynamic DMA mode (**Figure 9b**). The CNT/EVA fiber underwent six heating-cooling cycles at 0.15 MPa between 20 °C and 80 °C. The R_f and R_r for each heating-cooling cycle of the CNTs/EVA fiber were calculated. As can be seen in **Table 1**, the CNTs/EVA fiber has excellent shape memory performance in each heating-cooling cycle (both R_f and R_r are greater than 96%), which provides a theoretical basis for the self-repairing function of the CNTs/EVA fiber.

Firstly, the CNTs/EVA fiber underwent 1400 stretching-releasing cycles under 60% strain at 100 mm/min. As can be seen from **Figure 10a**, the prepared CNTs/EVA fiber has excellent dynamic stability and repeatability. However, it can also be found that the CNTs/EVA fiber produces an irreversible deformation after underwent 1400 cycles of stretching-releasing due to the viscoelasticity (**Figure 10b-c**). The conductivity of the CNTs/EVA fiber decreased from 2.650 S/m to 1.565 S/m, thus permanently destroying the conductive network. In order to evaluate the self-repairing function of CNTs/EVA fiber strain sensors, the CNTs/EVA fiber are placed in an oven at 70 °C for 5 min and then cooled to room temperature. It can be found that the irreversible deformation disappears and the electrical conductivity of the CNTs/EVA fiber returns to 2.646 S/m (**Figure 10d**). The self-repairing CNTs/EVA fiber underwent 1400 cycles of stretching-releasing under 60% strain. From the **Figure 10e**, it can be

found that the self-repairing of the CNTs/EVA fiber not only have excellent dynamic stability and repeatability but also have the same relative resistance as the original CNTs/EVA fiber at 60% strain. This shows that the CNTs/EVA fiber has excellent self-repairing performance, the problem of the sensors failure caused by the viscoelasticity of the elastic polymer can be solved, which dramatically improves the service life of the flexible strain sensors. Moreover, the thermal repair of the CNTs/EVA fiber was subjected to cyclic stretching-releasing with different strains (5%-50%) at a rate of 30 mm/min. It can be seen from the **Figure 10f** that the relative resistance of the thermal repaired CNTs/EVA fiber under different strains is basically the same as the relative resistance of the original CNTs/EVA fiber, we also found that the mechanical properties and sensitivity of the thermal repaired CNTs/EVA fiber are almost the same as the original CNTs/EVA (as shown in **Figure S2**), further verify that the CNTs/EVA fiber has outstanding self-repairing performance. The method of using the CNTs/EVA fiber shape memory to achieve repair is not only simple, but also has high repair efficiency, paving the way for the application in wearable devices.

In order to vividly show the change of electrical resistance of the CNTs/EVA fiber during stretching, we used the CNTs/EVA fiber and LED in series to form a simple circuit (operating voltages 10 V). It can be found that the brightness of the LED was enormous in the original position (**Figure 11a**), which showed that the CNTs/EVA fiber could work normally at 10 V voltage. It can be found that the brightness of the LED gradually decreases when the tensile strain increased from 0% to 100% (**Figure 11a-c**). It was because the conductive network of the CNTs is gradually damaged as the tensile strain increases, resulting in a decrease in the brightness of the LED. More interestingly,

the brightness of the LED gradually increased and returned to the original brightness when the CNTs/EVA fiber was released from 100% to 0% (**Figure 11d**), indicating the reconstruction of the conductive network causes the resistance to return to the original value, which is consistent with the sensing mechanism (**Figure 5b)**.

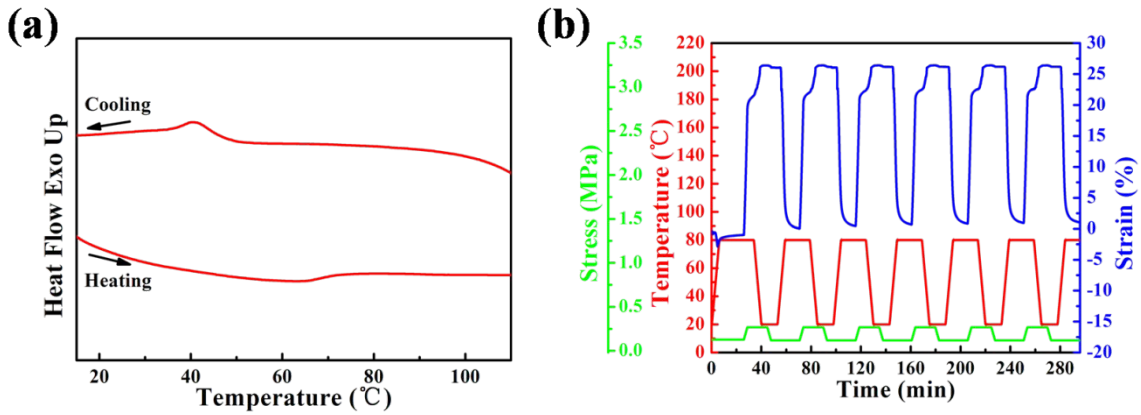

Figure 9. (a) DSC curves of CNTs/EVA fiber. (b) Shape memory property of CNTs/EVA fiber.

Table 1. Shape memory property of CNTs/EVA fiber

Cycles (*N*)	R_f (%)	R_r (%)
1	98.61	96.25
2	99.20	97.71
3	99.10	99.10
4	99.05	99.42
5	99.10	99.57
6	99.10	99.78

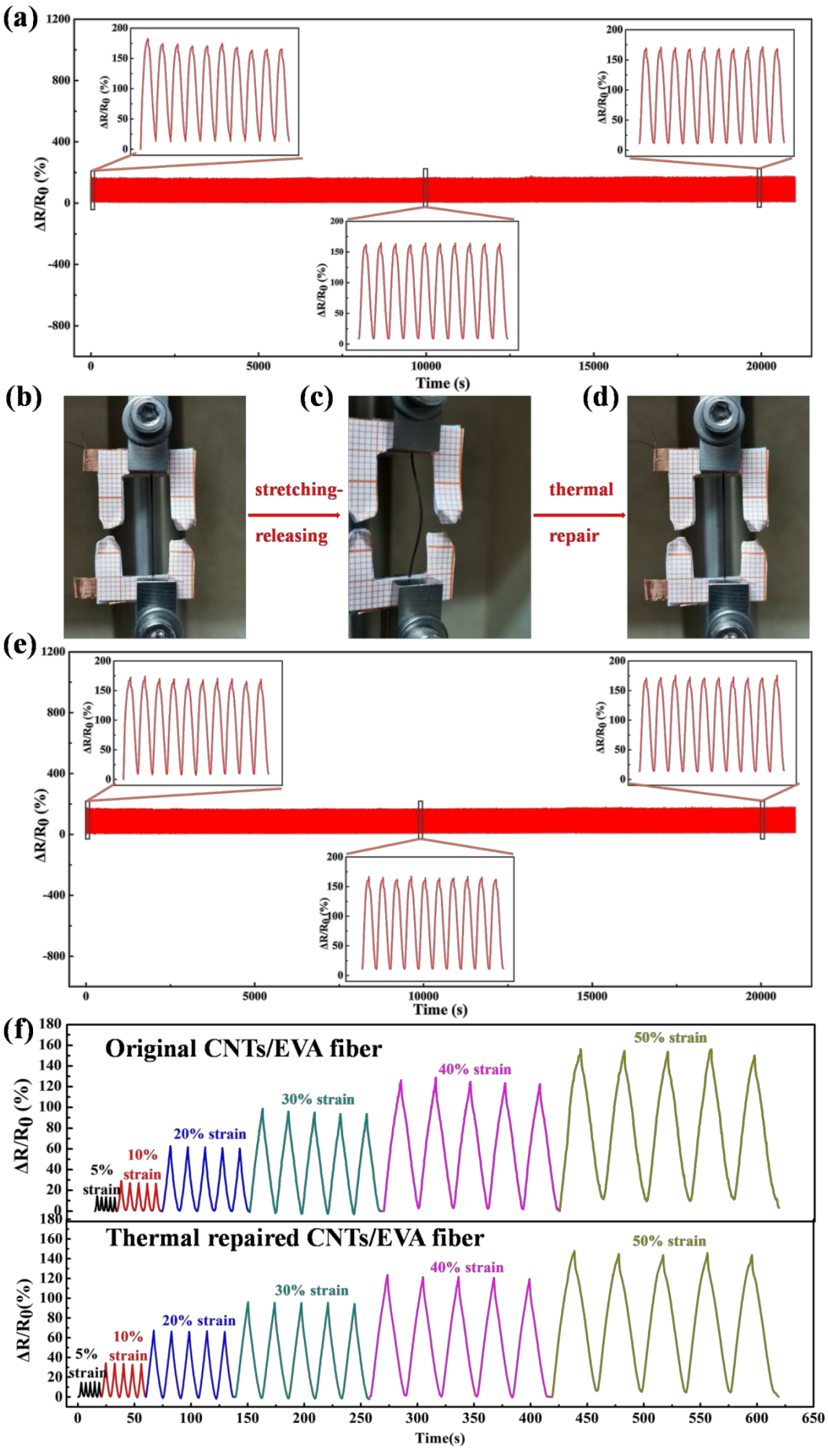
(a)
ΔR/R0 (%)
Time (s)
(b)
(c)
(d)
stretching-releasing
thermal repair
(e)
ΔR/R0 (%)
Time (s)
(f)
Original CNTs/EVA fiber
Thermal repaired CNTs/EVA fiber
ΔR/R0 (%)
5% strain
10% strain
20% strain
30% strain
40% strain
50% strain
Time(s)

Figure 10. (a) Cyclic stretching-releasing of CNTs/EVA fiber sensors under 60% strain at 100 mm/min for 1400 cycles. Digital images of CNTs/EVA fiber at different states: (b) the state of the original. (c) the state of after 1400 stretching-releasing cycles. (d) the state of after thermal treatment. (e) The self-repairing CNTs/EVA fiber strain sensors were subjected to 1400 cycles of stretch-release under 60% strain at 100 mm/min. (f) Relative resistance changes of the original and thermal repaired CNTs/EVA fiber with different strains at 30 mm/min.

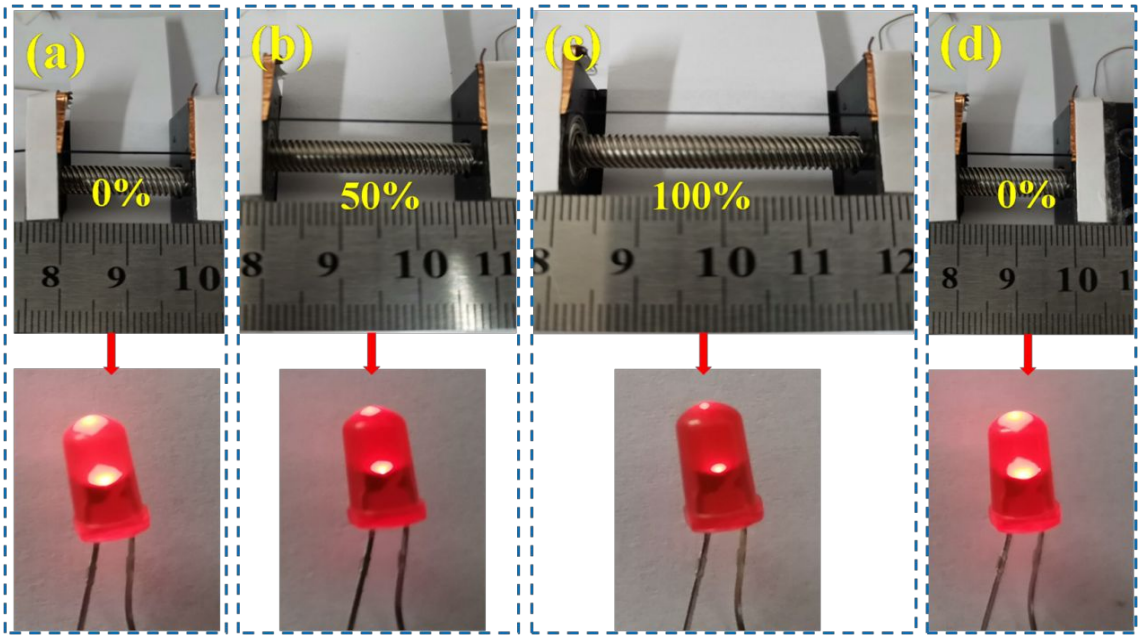

Figure 11. (a-d) Photograph of LED corresponding to CNTs/EVA fiber in different strains .

3.7 Human motion monitoring

The CNTs/EVA fiber has the advantages of good flexibility, fast response speed, excellent dynamic durability, self-repairing function, and a large linear working range. It is greatly suitable for monitoring human movements. The application of the CNTs/EVA fiber strain sensors in human movement monitoring is shown in **Figure**

12a-f. In order to evaluate the application of the CNTs/EVA fibers strain sensors in human health monitoring, the CNTs/EVA fibers are directly attached to the skin through the medical tape to monitor human movement. As shown in **Figure 12a**, the relative resistance of the CNTs/EVA fiber strain sensors gradually increases with bending and the relative resistance recover to its original value when the finger joint returns to the straightened state. The sensing signal shows that it is almost synchronized with the movement of the finger joint. **Figure 12b** shows the monitoring of the flexion movement of the wrist with CNTs/EVA fiber adhered to the wrist. Compared with fingers, the wrist has less bending deformation, resulting in a smaller change in relative resistance. Besides, the CNTs/EVA fiber can be installed on the elbow to detect and distinguish flatting-bending movements (**Figure 12c**). The transition between the elbow flexion and the flat state produces a greater displacement, causing the relative resistance of the elbow flexion to be larger. Therefore, we can accurately track the finger joint, wrist, and elbow flexion by monitoring the relative resistance. These results show that the CNTs/EVA fiber strain sensors can accurately detect human motion monitoring and have great application prospects in wearable devices.

In addition to monitoring large movement at joints, the CNTs/EVA fiber strain sensors can also be used to monitor subtle movements such as mouse clicks and pulse beat benefiting from excellent piezoresistive performance in a small range of strain. The CNTs/EVA fiber strain sensors were attached to the finger. During the quick click of the mouse, the relative resistance of the sensors is also rapidly and accurately recorded, and it can be seen that the sensors show repeatable, stable, and synchronized click mouse action response (**Figure 12d**). If the CNTs/EVA fiber strain sensors were fixed

on the wrist, it could also monitor human pulse caused by blood pressure under normal conditions. It can be found that valuable physiological signals of heart rate are accurately recorded in real-time, and the heart rate of the test volunteers is 70 beats/min (as shown in **Figure 12e**). The CNTs/EVA fiber strain sensors can also display typical human pulse characteristic peaks and the three peaks correspond to P-wave, T-wave, and D-wave (**Figure 12f**). The above results confirm that the CNTs/EVA fiber strain sensors exhibit excellent repeatability and stability in human motion monitoring. The sensors can detect not only large movements such as joint movement, but also detect subtle human movements including mouse clicks and pulses, showing their extremely application potentials in wearable devices, health monitoring, and smart products.

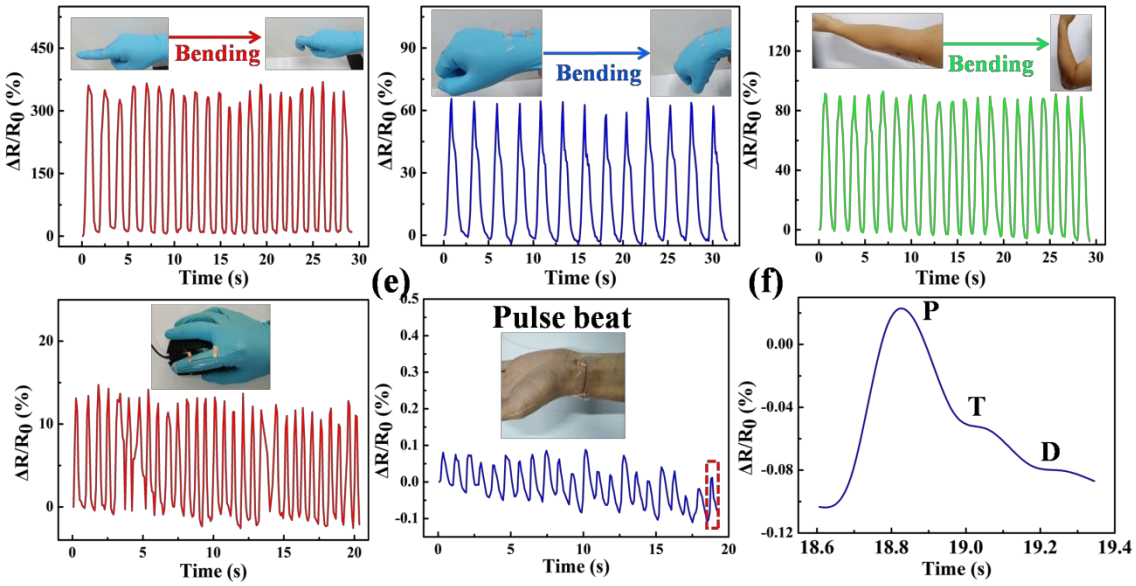

Figure 12. The application in human health monitoring for CNTs/EVA fiber strain sensors. The changes of relative resistance of CNTs/EVA fiber strain sensors attached to (a) the finger, (b) the wrist, and (c) the elbow under bending. (d) Response curve of CNTs/EVA fiber strain sensors to mouse click. (e) Relative resistance of CNTs/EVA fiber strain sensors attached to the wrist to monitor the wrist pulse. (f) The enlarged

view of the red area in (e).

4. CONCLUSIONS

In summary, a novel core-shell structure CNTs/EVA shape memory fiber-based flexible strain sensors were prepared via the swelling-ultrasonic method. The CNTs embed in the EVA fibers and overlap each other to form a unique and perfect embedded conductive network of the sensors. The stretchability, linear working range, dynamic durability, and response speed of the sensors can reach 190%, 88%, 5000 cycles, and 312 ms, respectively. Moreover, the permanently damage conductive network of the sensors caused by the irreversible deformation of the CNTs/EVA fiber after multiple stretching-relaxing cycles can be repaired by thermal treatment due to the excellent shape memory property of the cross-linked EVA fiber. The new type of self-repairing mechanism proposed in this work based on the shape memory effect of the polymer fiber endows the flexible strain sensors with fast repair and high repair efficiency. Furthermore, the CNTs/EVA fiber strain sensors can be used to monitor large movement at joints and subtle movements such as mouse clicks and pulse beats. Combine with other advantages: simple preparation, novel and efficient repair method, small size, lightweight, excellent flexibility, stitchability, and large-scale production, which demonstrated that the CNTs/EVA fiber strain sensors have wide application prospects in wearable devices.

SUPPORTING INFORMATION

Figure S1: Schematic of the formation mechanism of CNTs/EVA fiber.

Figure S2: (a) Stress-strain curves of CNTs/EVA fiber before and after thermal repair. (b) Relative resistance change of the thermal repaired CNTs/EVA fiber strain sensors vs strain.

Movie 1: CNTs adhesion testing.

ACKNOWLEDGMENTS

This work was supported by the National Natural Science Foundation of China (Grant No.5170324), Zhejiang Provincial Natural Science Foundation of China (Grant No. LY19E030010). National Training Programs of Innovation and Entrepreneurship for Undergraduates (Grant No. 201910338006), and Science Foundation of Zhejiang Sci-Tech University (Grant No. 19012179-Y).

REFERENCES

(1) Zou, B. H.; Chen, Y. Y.; Liu, Y. H.; Xie, R. J.; Du, Q. J.; Zhang, T.; Shen, Y.; Zheng, B.; Li, S.; Wu, J. S.; Zhang, W. N.; Huang, W.; Huang, X.; Huo, F. W. Repurposed Leather with Sensing Capabilities for Multifunctional Electronic Skin. *Adv. Sci.* **2019**, 6, No. 1801283.

(2) Dai, Y. T.; Fu, Y. M.; Zeng, H.; Xing, L. L.; Zhang, Y.; Zhan, Y.; Xue, X. Y. A

Self-Powered Brain-Linked Vision Electronic-Skin Based on Triboelectric-Photodetecing Pixel-Addressable Matrix for Visual-Image Recognition and Behavior Intervention. *Adv. Func. Mater*. **2018**, 28, No. 1800275.

(3) Lei, Z. Y.; Wang, Q. K.; Wu, P. Y. A Multifunctional Skin-Like Sensor Based on A 3D Printed Thermo-Responsive Hydrogel. *Mater. Horiz.* **2017**, 4, 694−700.

(4) Yang, Z.; Wang, D. Y.; Pang, Y.; Li, Y. X.; Wang, Q.; Zhang, T. Y.; Wang, J. B.; Liu, X.; Yang, Y. Y.; Jian, J. M.; Jian, M. Q.; Zhang, Y. Y.; Yang, Y.; Ren, T. L. Simultaneously Detecting Subtle and Intensive Human Motions Based on a Silver Nanoparticles Bridged Graphene Strain Sensor. *ACS Appl. Mater. Interfaces* **2018**, 10, 3948–3954.

(5) Lee, H.; Glasper, M. J.; Li, X. D.; Nychka, J. A.; Batcheller, J.; Chung, H. J.; Chen, Y. Preparation of Fabric Strain Sensor Based on Graphene for Human Motion Monitoring. *J. Mater. Sci.* **2018**, 53, 9026–9033.

(6) Sun, S. B.; Guo, L.; Chang, X. T.; Liu, Y. Q.; Niu, S. C.; Lei, Y. H.; Liu, T.; Hu, X. A Wearable Strain Sensor Based on the ZnO/Graphene Nanoplatelets Nanocomposite with Large Linear Working Range. *J. Mater. Sci.* **2019**, 54, 7048–7061.

(7) Wang, Y. L.; Hao, J.; Huang, Z. Q.; Zheng, G. Q.; Dai, K.; Liu, C. T.; Shen, C. Y. Flexible Electrically Resistive-Type Strain Sensors Based on Reduced Graphene Oxide-Decorated Electrospun Polymer Fibrous Mats for Human Motion Monitoring. *Carbon* **2018**, 126, 360−371.

(8) Amjadi, M.; Turan, M.; Clementson, C. P.; Sitti, M. Parallel Microcracks-Based

Ultrasensitive and Highly Stretchable Strain Sensors. *ACS Appl. Mater. Interfaces* **2016**, 8, 5618−5626.

(9) Kim, J. Y.; Ji, S.; Jung, S.; Ryu, B. H.; Kim, H. S.; Lee, S. S.; Choi, Y.; Jeong, S. 3D Printable Composite Dough for Stretchable, Ultrasensitive and Body-Patchable Strain Sensors. *Nanoscale* **2017**, 9, 11035−11046.

(10) Amjadi, M.; Kyung, KU.; Park, I.; Sitti, M.; Stretchable, Skin-Mountable, and Wearable Strain Sensors and Their Potential Applications: A Review. *Adv. Funct. Mater*. **2016**, 26, 1678–1698.

(11) Zheng, Y. J.; Li, Y. L.; Li, Z. Y.; Wang, Y. L.; Dai, K.; Zheng, G. Q.; Liu, C. T.; Shen, C. Y. The Effect of Filler Dimensionality on the Electromechanical Performance of Polydimethylsiloxane Based Conductive Nanocomposites for Flexible Strain Sensors. *Compos. Sci. Technol.* **2017**, 139, 64–73.

(12) Wei, P. Q.; Yang, X.; Cao, Z. M.; Guo, X. L.; Jiang, H. L.; Chen, Y.; Morikado, M.; Qiu, X. B.; Yu, D. L. Flexible and Stretchable Electronic Skin with High Durability and Shock Resistance via Embedded 3D Printing Technology for Human Activity Monitoring and Personal Healthcare. *Adv Mater Technol-US.* **2019**, 4, No.1900315.

(13) Xu, M. X.; Li, F.; Zhang, Z. Y.; Shen, T.; Zhang, Q.; Qi, J. J. Stretchable and Multifunctional Strain Sensors Based on 3D Graphene Foams for Active and Adaptive Tactile Imaging. *Sci. China Mater*. **2019**, 62, 555–565.

(14) Zheng, Y. J.; Li, Y. L.; Dai, K.; Liu, M. R.; Zhou, K. K.; Zheng, G. Q.; Liu, C. T.; Shen, C. Y. Conductive Thermoplastic Polyurethane Composites with Tunable

Piezoresistivity by Modulating the Filler Dimensionality for Flexible Strain Sensors. *Compos Part A-Appl S*. **2017**, 101, 41–49.

(15) Dong, X. C.; Wei, Y.; Chen, S.; Lin, Y.; Liu, L.; Li, J. A Linear and Large-Range Pressure Sensor Based on a Graphene/Silver Nanowires Nanobiocomposites Network and a Hierarchical Structural Sponge. *Compos. Sci. Technol.* **2018**, 155, 108–116.

(16) Kahn, N.; Lavie, O.; Paz, M.; Segev, Y.; Haick, H. Dynamic Nanoparticle-Based Flexible Sensors: Diagnosis of Ovarian Carcinoma from Exhaled Breath. *Nano Lett*. **2015**, 15, 7023−7028.

(17) Lu, L. J.; Wei, X. D.; Zhang, Y.; Zheng, G. Q.; Dai, K.; Liu, C. T.; Shen, C. Y. A Flexible and Self-Formed Sandwich Structure Strain Sensor Based on AgNW Decorated Electrospun Fibrous Mats with Excellent Sensing Capability and Good Oxidation Inhibition Properties. *J. Mater. Chem. C.* **2017**, 5, 7035−7042.

(18) Li, J. H.; Zhao, S. F.; Zeng, X. L.; Huang, W. P.; Gong, Z. Y.; Zhang, G. P.; Sun, R.; Wong, C. P. Highly Stretchable and Sensitive Strain Sensor Based on Facilely Prepared Three-Dimensional Graphene Foam Composite. *ACS Appl. Mater. Interfaces* **2016**, 8, 18954–18961.

(19) Chen, S.; Wei, Y.; Wei, S. M.; Lin, Y.; Liu, L. Ultrasensitive Cracking-Assisted Strain Sensors Based on Silver Nanowires/Graphene Hybrid Particles. *ACS Appl. Mater. Interfaces* **2016**, 8, 25563–25570.

(20) Li, Y. C.; Zheng, C. R.; Liu, S.; Huang, L.; Fang, T. S.; Li, J. X.; Xu, F.; Li, F. Smart Glove Integrated with Tunable MWNTs/PDMS Fiber Made of a One-Step

Extrusion Method for Finger Dexterity, Gesture, and Temperature Recognition. *ACS Appl. Mater. Interfaces* **2020**, 12, 23764–23773.

(21) Gao, J. C.; Wang, X. Z.; Zhai, W.; Liu, H.; Zheng, G. Q.; Dai, K.; Mi, L. W.; Liu, C. T.; Shen, C. Y. Ultrastretchable Multilayered Fiber with a Hollow-Monolith Structure for High-Performance Strain Sensor. *ACS Appl. Mater. Interfaces* **2018**, 10, 34592–34603.

(22) Huang, W. J.; Dai, K.; Zhai, Y.; Liu, H.; Zhan, P. F.; Gao, J. C.; Zheng, G. Q.; Liu, C. T.; Shen, C. Y. Flexible and Lightweight Pressure Sensor Based on Carbon Nanotube/Thermoplastic Polyurethane-Aligned Conductive Foam with Superior Compressibility and Stability. *ACS Appl. Mater. Interfaces* **2017**, 9, 42266–42277.

(23) Yang, Y.; Zhu, B. P.; Yin, D.; Wei, J. H.; Wang, Z. Y.; Xiong, R.; Shi, J.; Liu, Z. Y.; Lei, Q. Q. Flexible Self-Healing Nanocomposites for Recoverable Motion Sensor. *Nano Energy* **2015**, 17, 1–9.

(24) Bai, S. L.; Sun, C. Z.; Yan, H.; Sun, X. M.; Zhang, H.; Luo, L.; Lei, X. D.; Wan, P. B.; Chen, X. D. Healable, Transparent, Room-Temperature Electronic Sensors Based on Carbon Nanotube Network-Coated Polyelectrolyte Multilayers. *Small* **2015**, 11, 5807–5813.

(25) Liu, S. Q.; Lin, Y.; Wei, Y.; Chen, S.; Zhu, J. R.; Liu, L. A High Performance Self-Healing Strain Sensor with Synergetic Networks of Poly (Esilon-Caprolactone) Microspheres, Graphene and Silver Nanowires. *Compos. Sci. Technol.* **2017**, 146, 110–118.

(26) Liu, S. J.; Li, L. Ultrastretchable and Self-Healing Double-Network Hydrogel for 3D Printing and Strain Sensor. *ACS Appl. Mater. Interfaces* **2017**, 9, 26429–26437.

(27) Li, J. H.; Liu, Q.; Ho, D.; Zhao, S. F.; Wu, S. W.; Ling, L.; Han, F.; Wu, X. X.; Zhang, G. P.; Sun, R.; Wong, C. P. Three-Dimensional Graphene Structure for Healable Flexible Electronics Based on Diels-Alder Chemistry. *ACS Appl. Mater. Interfaces* **2018**, 10, 9727–9735.

(28) Yang, B.; Xuan, F. Z.; Wang, Z. Q.; Chen, L. M.; Lei, H. S.; Liang, W. Y.; Xiang, Y. X.; Yang, K. Multi-Functional Interface Sensor with Targeted IFSS Enhancing, Interface Monitoring and Self-Healing of GF/EVA Thermoplastic Composites. *Compos. Sci. Technol.* **2018**, 167, 86–95.

(29) Rahaman, M.; Chaki, T. K.; Khastgir, D. Polyaniline, Ethylene Vinyl Acetate Semi-Conductive Composites as Pressure Sensitive Sensor. *J Appl Polym Sci*. **2013**, 128 (1), 161–168.

(30) Sun, L.; Wang, T. X.; Chen, H. M.; Salvekar, A. V.; Naveen, B. S.; Xu, Q.; Weng, Y.; Guo, X.; Chen, Y.; Huang, W. M. A Brief Review of the Shape Memory Phenomena in Polymers and Their Typical Sensor Applications. *Polymers* **2019**, 11, No. 1049.

(31) Besse, N.; Rosset, S.; Zarate, J. J.; Shea, H. Flexible Active Skin: Large Reconfigurable Arrays of Individually Addressed Shape Memory Polymer Actuators. *Adv Mater Technolo-US*. **2017**, 2, No.1700102.

(32) Castano, L. M.; Flatau, A. B. Smart Fabric Sensors and E-Textile Technologies: A

review. *Smart. Mater. Struct.* **2014**, 23, No. 053001.

(33) Yip, M. C.; Niemeyer, G. On the Control and Properties of Supercoiled Polymer Artificial Muscles. *IEEE Trans. Robot* **2017**, 33, 689–699.

(34) Imran, M.; Zhang, X. X. Ferromagnetic Shape Memory Ni-Fe-Ga Alloy Foams for Elastocaloric Cooling. *J. Phys. D. Appl. Phys.* **2020**, 53, 245503.

(35) Yao, Y.; Zhou, T.; Xu, Y.; Liu, Y.; Leng, J. Preparation and Characterization of Shape Memory Composite Foams Based on Solid Foaming Method. *J. Appl. Polym. Sci*. **2018**, 135, No. 46767.

(36) Wang, E. L.; Dong, Y. B.; Islam, M. Z.; Yu, L. M.; Liu, F. Y.; Chen, S. J.; Qi, X. M.; Zhu, Y. F.; Fu, Y. Q.; Xu, Z. H.; Hu, N. Effect of Graphene Oxide-Carbon Nanotube Hybrid Filler on the Mechanical Property and Thermal Response Speed of Shape Memory Epoxy Composites. *Compos. Sci. Technol*. **2019**, 169, 209–216.

(37) Dong, Y. B.; Xia, H.; Zhu, Y. F.; Ni, Q. Q.; Fu, Y. Q. Effect of Epoxy-Graft-Polyoxyethylene Octyl Phenyl Ether on Preparation, Mechanical Properties and Triple-Shape Memory Effect of Carbon Nanotube/Water-Borne Epoxy Nanocomposites. *Compos. Sci. Technol*. **2015**, 120, 17–25.

(38) Qi, X. M.; Yang, W. T.; Yu, L. M.; Wang, W. J.; Lu, H. H.; Wu, Y. L.; Zhu, S. W.; Zhu, Y. F.; Liu, X. D.; Dong, Y. B.; Fu, Y. Q. Design of Ethylene-Vinyl Acetate Copolymer Fiber with Two-Way Shape Memory Effect. *Polymers* **2019**, 11, No. 1599.

(39) Aslan, S.; Kaplan, S. Thermomechanical and Shape Memory Performances of Thermo-Sensitive Polyurethane Fiber. *Fiber Polym*. **2018**, 19, 272–280.

(40) Qian, C.; Dong, Y. B.; Zhu, Y. F.; Fu, Y. Q. Two-Way Shape Memory Behavior of Semi-Crystalline Elastomer under Stress-Free Condition. *Smart. Mater. Struct.* **2016**, 25, No. 085023.

(41) Qian, C.; Zhu, Y. F.; Dong, Y. B.; Fu, Y. Q. Vapor-Grown Carbon Nanofiber/Poly (Ethylene-Co-Vinyl Acetate) Composites with Electrical-Active Two-Way Shape Memory Behavior. *J. Intell. Mater. Syst. Struct*. **2017**, 28, 2749–2756.

(42) Fang, T. Y.; Cao, L. L.; Chen, S. P.; Fang, J. J.; Zhou, J.; Fang, L.; Lu, C. H.; Xu, Z. Z. Preparation and assembly of five photoresponsive polymers toachieve complex light-induced shape deformations. *Mater. Design* **2018**, 144, 129-139.

(43) Zhou, C. H.; Ni, Y. R.; Liu, W. T.; Tan, B.; Yao, M. C.; Fang, L.; Lu, C. H.; Xu, Z. Z. Near-Infrared Light-Induced Sequential Shape Recovery and Separation of Assembled Temperature Memory Polymer Microparticles. *Macromol. Rapid Comm.* **2020**, 41, No. 2000043.

(44) Sun, F. Q.; Tian, M. W.; Sun, X. T.; Xu, T. L.; Liu, X. Q.; Zhu, S. F.; Zhang, X. J.; Qu, L. J. Stretchable Conductive Fiber of Ultrahigh Tensile Strain and Stable Conductance Enabled by a Worm-Shaped Graphene Microlayer. *Nano Lett.* **2019**, 19, 6592–6599.

(45) Zhao, L.; Qiang, F.; Dai, S. W.; Shen, S. C.; Huang, Y. Z.; Huang, N. J.; Zhang, G. D.; Guan, L. Z.; Gao, J. F.; Song, Y. H.; Tang, L. C. Construction of Sandwich-Like Porous Structure of Graphene-Coated Foam Composites for Ultrasensitive and Flexible Pressure Sensors. *Nanoscale* **2019**, 11, 10229–10238.

(46) Montazerian, H.; Rashidi, A.; Dalili, A.; Najjaran, H.; Milani, A. S.; Hoorfar, M. Graphene-Coated Spandex Sensors Embedded into Silicone Sheath for Composites Health Monitoring and Wearable Applications. *Small* **2019**, 15, No. 1804991.

(47) Fu, Y. F.; Li, Y. Q.; Liu, Y. F.; Huang, P.; Hu, N.; Fu, S. Y. High-Performance Structural Flexible Strain Sensors Based on Graphene-Coated Glass Fabric/Silicone Composite. *ACS Appl. Mater. Interfaces* **2018**, 10, 35503–35509.

(48) Luo, B.; Wei, Y.; Chen, H. L.; Zhu, Z. C.; Fan, P.; Xu, X. J.; Xie, B. J. Printing Carbon Nanotube-Embedded Silicone Elastomers via Direct Writing. *ACS Appl. Mater. Interfaces* **2018**, 10, 44796–44802.

(49) Wang, Z. H.; Zhang, L.; Duan, S. S.; Jiang, H.; Shen, J. H.; Li, C. Z. Kirigami-Patterned Highly Stretchable Conductors from Flexible Carbon Nanotube-Embedded Polymer Films. *J. Mater. Chem. C.* **2017**, 5, 8714–8722.

(50) Jiang, D.; Wang, N.; Edwards, M.; Mu, W.; Nylander, A.; Fu, Y. F.; Jeppson, K.; Liu, J. H. Embedded Fin-Like Metal/CNT Hybrid Structures for Flexible and Transparent Conductors. *Small* **2016**, 12, 1521–1526.

(51) Gu, J.; Kwon, D.; Ahn, J.; Park, I. Wearable Strain Sensors Using Light Transmittance Change of Carbon Nanotube-Embedded Elastomers with Microcracks. *ACS Appl. Mater. Interfaces* **2020**, 12, 10908–10917.

(52) Coleman, J. N.; Khan, U.; Gun'ko, Y. K.; Mechanical Reinforcement of Polymers Using Carbon Nanotubes. *Adv. Mater*. **2006**, 18, 689–706.

(53) Gao, J. F.; Hu, M. J.; Dong, Y. C.; Li, RKY. Graphite-Nanoplatelet-Decorated

Polymer Nanofiber with Improved Thermal, Electrical, and Mechanical Properties. *ACS Appl. Mater. Interfaces* **2013**, 5, 7758–7764.

(54) Liu, H.; Gao, J. C.; Huang, W. J.; Dai, K.; Zheng, G. Q.; Liu, C. T.; Shen, C. Y.; Yan, X. R.; Guo, J.; Guo, Z. H. Electrically Conductive Strain Sensing Polyurethane Nanocomposites with Synergistic Carbon Nanotubes and Graphene Bifillers. *Nanoscale* **2016**, 8, 12977–12989.

TOC graphic

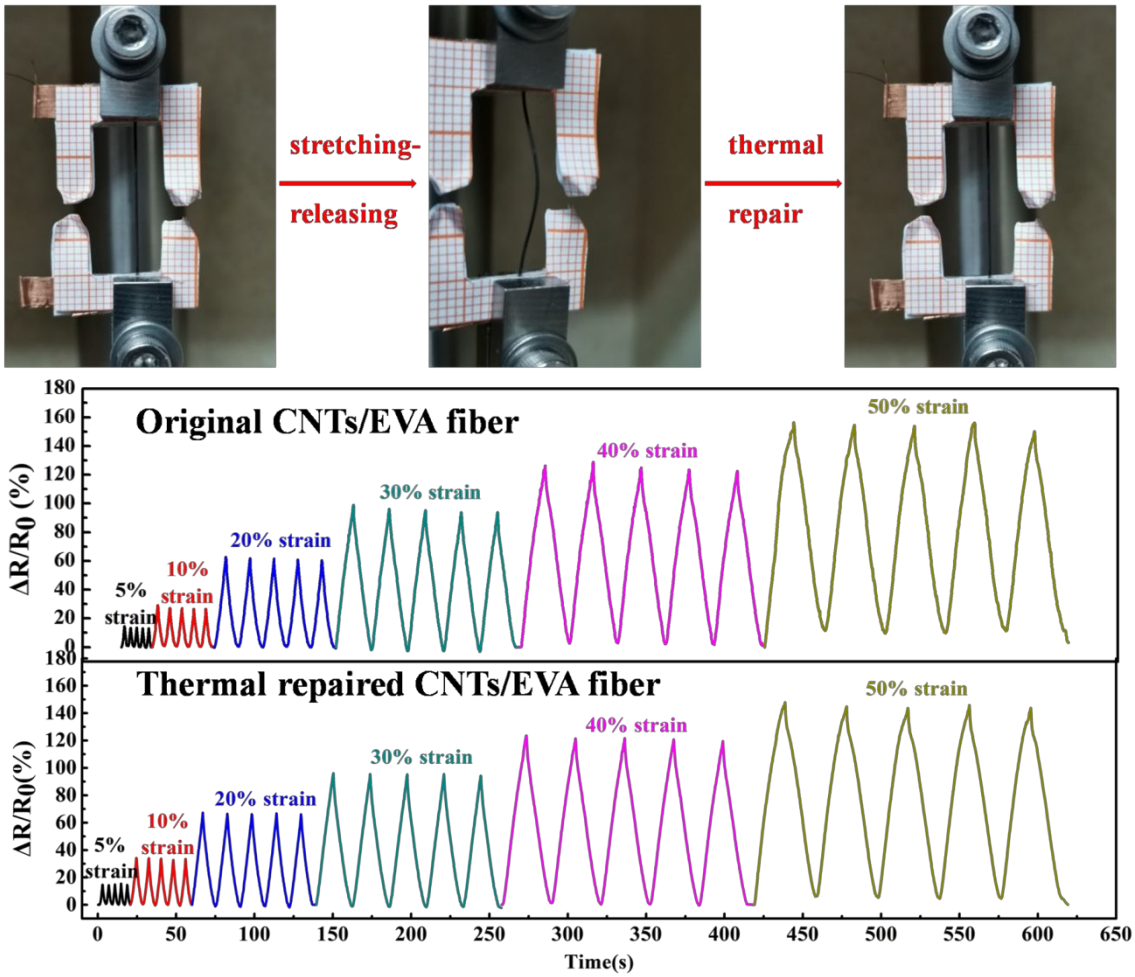
stretching-
releasing
thermal
repair
Original CNTs/EVA fiber
Thermal repaired CNTs/EVA fiber
ΔR/R0 (%)
5% strain
10% strain
20% strain
30% strain
40% strain
50% strain
Time(s)